Laboratory measurements of limiting freak waves on currents

Chin H. Wu and Aifeng Yao

Department of Civil and Environmental Engineering, University of Wisconsin-Madison, Madison, Wisconsin, USA

Received 20 July 2004; revised 27 September 2004; accepted 11 October 2004; published 3 December 2004.

[1] The results of laboratory measurements on limiting freak waves in the presence of currents are reported. Both dispersive spatial-temporal focusing and wave-current interaction are used to generate freak waves in a partial random wave field in the presence of currents. Wave group structure, for example, spectral slope and frequency bandwidth, is found to be critical to the formation and the geometric properties of freak waves. A nondimensional spectral bandwidth is shown to well represent wave group structure and proves to be a good indicator in determining limiting freak wave characteristics. The role of a co-existing current in the freak wave formation is recognized. Experimental results confirm that a random wave field does not prevent freak wave formation due to dispersive focusing. Strong opposing currents inducing partial wave blocking significantly elevate the limiting steepness and asymmetry of freak waves. At the location where a freak wave occurs, the Fourier spectrum exhibits local energy transfer to high-frequency waves. The Hilbert-Huang spectrum, a time-frequency-amplitude spectrum, depicts both the temporal and spectral evolution of freak waves. A strong correlation between the magnitude of interwave instantaneous frequency modulation and the freak wave nonlinearity (steepness) is observed. The experimental results provide an explanation to address the occurrence and characteristic of freak waves in consideration of the onset of wave breaking. *INDEX TERMS:* 4504 Oceanography: Physical: Air/sea interactions (0312); 4546 Oceanography: Physical: Nearshore processes; 4560 Oceanography: Physical: Surface waves and tides (1255); 4572 Oceanography: Physical: Upper ocean processes; *KEYWORDS:* freak waves, rogue waves, dispersive focusing, wave-current interaction, time-frequency analysis, Hilbert-Huang Transformation (HHT)

Citation: Wu, C. H., and A. Yao (2004), Laboratory measurements of limiting freak waves on currents, *J. Geophys. Res.*, *109*, C12002, doi:10.1029/2004JC002612.

1. Introduction

[2] Freak waves, alternatively called rogue waves or giant waves, are exceptionally large, steep, and asymmetric waves whose heights usually exceed by 2.2 times the significant wave height [*Dean*, 1990]. They have also been described as "holes in the sea" or "walls of waters" [*Draper*, 1965; *Mallory*, 1974; *Kjeldsen*, 1984; *Sand et al.*, 1990; *Yasuda and Mori*, 1997; *Lavrenov*, 1998; *Chien et al.*, 2002]. These waves have been long known to be notorious hazards to navigation vessels and marine structures. Many sinister marine episodes and their devastating impacts have prompted a great interest in freak waves. With little warning, freak waves often mysteriously occur as transient giant waves from wave groups in random coastal and open seas [*Pelinovsky et al.*, 2000; *Slunyaev et al.*, 2002; *Peterson et al.*, 2003]. Statistical methods are widely employed in examining the occurrence of such extreme sea conditions [*Forristall*, 1984; *Sand et al.*, 1990; *Yasuda and Mori*, 1997; *Chien et al.*, 2002; *Mori et al.*, 2002; *Mori*, 2004]. However, as recently addressed by *Haver and Andersen* [2000], it is still unclear whether freak waves are a rare realization of a typical population or a typical realization of a rare population. A recent work by *Liu and Pinho* [2004] even found that the occurrence of freak waves is actually more frequent than rare. *Kharif and Pelinovsky* [2003] suggested that the productivity of statistical method could be limited due to the rare feature of freak waves. Likewise, it is unclear whether wave breaking (limiting wave condition) and the role of currents can affect the extreme wave statistics. As suggested by *Janssen* [2003], deterministic studies of limiting freak wave steepness are needed to carefully justify the statistical descriptions of the freak wave heights. Therefore it is crucial to have a fundamental understanding of the physical mechanisms of freak wave formation and its limiting characteristics.

[3] Over the past 2 decades, observations have helped us to gain remarkable knowledge on freak waves. An excellent review of freak waves is given by *Kharif and Pelinovsky* [2003]. Several mechanisms have been suggested as possible causes for freak waves. In areas where there are spatially nonuniform currents, the wave-current interaction could concentrate wave energy in a small area due to reflection and/or refraction [*Peregrine*, 1976; *Smith*, 1976; *Lavrenov*, 1998]. Variable bathymetry that can spatially focus wave energy can also create freak waves. Both these two mechanisms are sometimes known as geometric or spatial focusing. Far away from variable currents or bathymetry, a nonlinear mechanism of a narrowband, deep-water wave

0148-0227/04/2004JC002612$09.00

train may undergo the modulation or Benjamin-Feir instability [*Benjamin and Feir*, 1967] to self-focusing a nonlinear wave train for forming freak waves, which have been extensively investigated analytically and numerically [*Trulsen and Dysthe*, 1997; *Henderson et al.*, 1999; *Dysthe and Trulsen*, 1999; *Osborne et al.*, 2000; *Onorato et al.*, 2001, 2002], as well as in the laboratory [*Lake et al.*, 1977; *Su et al.*, 1982; *Tulin and Waseda*, 1999]. Another mechanism, dispersive spatial-temporal focusing, has been shown to effectively create freak waves through the superposition of different frequency wave components at a specific time and position [*Kharif et al.*, 2001]. This mechanism has been widely employed in the laboratory to successfully generate two- and three-dimensional, extreme waves or breaking waves [*Kjeldsen*, 1990; *Rapp and Melville*, 1990; *Baldock et al.*, 1996; *Nepf et al.*, 1998; *Johannessen and Swan*, 2001]. A combination of the dispersive-focusing and geometric-focusing mechanisms to form an extreme wave has also been examined [*Wu and Nepf*, 2002]. Furthermore, nonlinear wave-wave interaction has been addressed to associate with freak wave formation [*Mori and Yasuda*, 2002; *Janssen*, 2003]. Overall, these studies have provided us a good understanding or explanation to the mechanisms for freak wave formation.

[4] Nevertheless, previous studies have raised some questions that deserve further investigation. First, while the role of frequency bandwidth in extreme waves formed from focused wave groups has been addressed by *Stansberg* [1994], *Baldock et al.* [1996], and *Brown and Jensen* [2001], the limiting characteristics of these waves are not fully examined. *Onorato et al.* [2001] showed that the reduction in the frequency bandwidth (by increasing the value of the Phillips parameter and the enhancement coefficient in the JONSWAP spectrum) [*Komen et al.*, 1994] is more likely to promote freak waves through modulational instability. Their numerical simulations are based on the nonlinear Schrödinger (NLS) equation that formally assumes a narrow-banded frequency process. Therefore it is uncertain that in a broadbanded wave group under dispersive focusing, the correlation of freak wave occurrence with frequency bandwidth still holds. Second, to date, very limited attention has been paid to the interaction of a current and a focused wave group [*Thomas and Klopman*, 1997]. *Chen and Liu* [1976] analytically obtained an exact solution for describing a freak waveform under the balance of dispersive focusing (defocusing) and attenuation (amplification) in the zone of the nonuniform current. However, their solution for the zone or extent of a freak wave seems to be much wider, comparing with the one of quasi-monochromatic waves [*Kharif and Pelinovsky*, 2003]. While extreme and breaking waves on uniform currents have been studied in laboratory experiments [*Lai et al.*, 1989; *Bonmarin et al.*, 1995; *Chawla and Kirby*, 2002], the limiting waveforms before breaking in those situations have not yet been examined. Moreover, only monochromatic and irregular waves, rather than a focused wave group, were considered by these authors. Therefore, dispersive focusing of a wave group in the presence of a co-existing current remains to be investigated. Finally, experimental validations of the roles of random wave and weak current fluctuations in freak waves evolved from focused wave groups are still lacking [*Slunyaev et al.*, 2002; *White and Fornberg*, 1998; *Dysthe*, 2001]. As one can see, our understanding of the factors and mechanisms behind the occurrence of freak waves are not yet complete.

[5] This study is motivated by the desire to address the above-mentioned issues. In particular, we are interested in further understanding the formation mechanisms, limiting characteristics, and temporal-spatial-spectral evolutions of freak waves on currents. In the following section, instrumentation and details of the experimental methods are described. Generation of freak waves in a laboratory flume under varying spectral slope (steep or mild), frequency bandwidth (broad or narrow), and co-existing currents (weak to strong, following or opposing) is illustrated. Freak waves on partial wave-blocking conditions due to strong opposing currents are examined. Random wave components are introduced into wave groups to assess their influence on freak wave formation due to dispersive focusing. In section 3, data analysis techniques are outlined. Results of the surface displacements, limiting wave geometries, spatial and temporal spectral evolutions using the Fourier transformation (FT) and the Hilbert-Huang transformation (HHT) [*Huang et al.*, 1998, 1999] are given in section 4. Finally, conclusions and recommendations are provided in section 5.

2. Experimental Methods

2.1. Instrumentation

[6] The experiment was conducted in a wave-current flume in the Environmental Fluid Mechanics Laboratory at University of Wisconsin, Madison. The flume is 46 m long, 0.91 m wide, and filled with tap water up to a depth of 0.6 m (Figure 1). A coordinate system is defined as the x axis in the wave propagation direction and the z axis vertically upward originating at the free surface. A level and smooth bed condition was maintained. A bottom-hinged wave-maker, capable of generating waves and absorbing reflected wave components by incorporating a force feedback mechanism, was located at one end of the flume. The transfer function between the wave-maker and observed surface displacement was determined using an impulse response method. At the other end of the flume, a slope of 1:10 absorption beach covered with wire mesh and a 4-inch-thick, porous horse mate was installed. The beach was tested to absorb 95% incoming monochromatic waves, based upon the three-gauge method [*Rosengaus Moshinsky*, 1987].

[7] Both following and opposing currents were achieved using a bidirectional centrifugal pump that drew water from a settling well behind the wave-maker to another settling well behind the absorptive beach through stainless steel spiral pipes. Following currents, in the same direction as wave propagation, were introduced through a sloping bed opening covered with a wire mesh in front of the wave-maker. Opposing currents were generated by reversing the pump to allow water to go through the beach. Current velocities were measured using a 16-MHz Sontek micro-acoustic Doppler velocimeter. The current profile was found to be essentially uniform in depth, about 35 cm, which is approximately 3.5 times the typical maximum wave height. Stream-wise variations of the mean velocity between $x = 4$ m to $x = 16$ m were less than 5%. The maximum turbulence intensity was less than 15%. These conditions allow us to

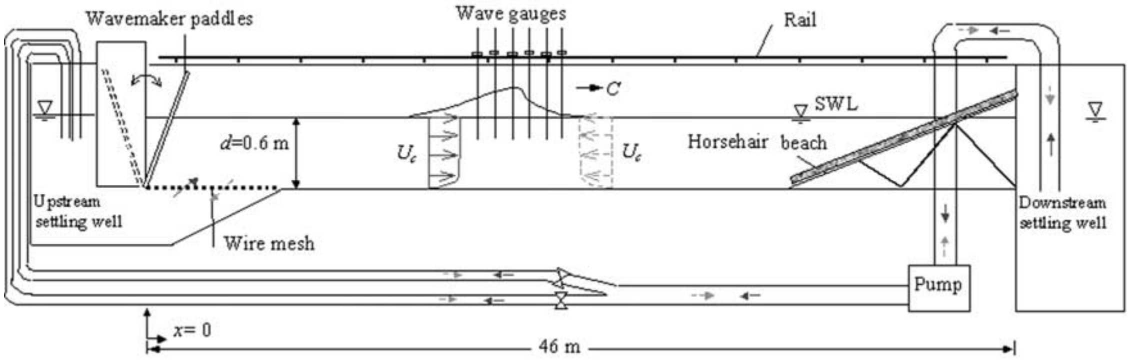

Figure 1. Schematic of the experimental setup. The wave-current flume consists of a bottom-hinged wave maker, a sloping opening with a wired mesh, an absorption beach, and a bidirectional pump with a recirculating pipeline.

justify the validity of using uniform currents interacting with waves.

[8] Water surface displacement was measured using six capacitance-type wave gauges, manufactured by Protecno S.R.L. in Italy, on a moving carriage system. A 12-bit data acquisition board (DAS1602, Keithley Instrument, Inc.) was used to record surface displacement at 200 Hz. Depending on the measurement span of the testing cases, at least 20 locations for each type of freak wave were conducted. A total sampling time of 70 s was chosen to allow for the passage of the groups at all measurement locations and to avoid any energetic reflections from the beach. Prior to generating waves on a current, a desired current was first created and elapsed at least 1 hour to achieve a steady state water level, upon which the calibration of wave gages was performed. The effect from the temperature heating the water in the pumping system on the thermal drifting of wave gauges could be significantly reduced. From preliminary tests, an accuracy of 0.5 mm was found using the measurements of the gauges.

[9] To record fast-deforming freak wave profiles, a high-speed X-Stream VISION XS-3 camera with a Nikon lens of 28 mm f/2.8 D-AF was used at a rate of 200 frames per second. The image size is 1260H × 1024V with 8-bit depth. To capture a large field of view (approximately 2 m area), a backlighted imaging technique was employed. A highly reflective, white panel was attached to the back sidewall of the flume and illuminated by a pair of 500-Watt halogen lights. The reflective panel served as a backlighting source for the water column, resulting in high contrast between air and water on images.

2.2. Freak Wave Generation

[10] In the laboratory, if a freak wave is simulated using a realistic wave spectrum (e.g., JONSWAP spectrum) with a random phase approach, this rare event would occur only once in approximately 3000 waves according to a Rayleigh wave height distribution. Therefore this method is not often adopted for freak wave laboratory experiments. Alternatively, spatial-temporal focusing of a wave group has been widely used to generate extreme or breaking waves in the laboratory [*Rapp and Melville*, 1990; *Nepf et al.*, 1998; *Glauss et al.*, 2002]. The method is based upon the concept that dispersion can focus different waves at a given position and time to form a large wave by arranging the initial phases of the frequency components in a wave group. For focusing a wave group on a current field, the effects of wave-current interaction [*Peregrine*, 1976] on wave modulation are important. In this study, we develop a new freak wave generation method involving both the mechanisms of dispersive focusing and wave-current interaction. In addition, we generate a focusing wave packet with a relatively narrow frequency bandwidth and examine the characteristics of the Benjamin-Feir instability in a focusing freak wave train. A description for generating freak waves on currents is given below.

[11] Free surface displacement, based on linear wave theory, can be specified by

$$\eta(x,t) = \sum_{n=1}^{N} a_n \cos(k_n x - \omega_n t + \theta_n), \tag{1}$$

where $N = 32$, the number of wave components, was chosen to achieve a smooth and continuous wave amplitude spectrum; k_n, ω_n, θ_n, and a_n denote the wave number, apparent radian frequency, phase, and amplitude of the nth wave component, respectively. For the effects of wave-current interaction, k_n is determined by solving the linear Doppler-shifted dispersion relation [*Peregrine*, 1976],

$$\omega_n = \sigma_n + k_n U = \sqrt{k_n g \tanh(k_n d)} + k_n U, \tag{2}$$

where g and d are the gravitational acceleration and water depth, and σ_n is the intrinsic (relative) wave frequency observed in a moving frame at the current velocity U. The sign of U is positive or negative depending on either following or opposing currents relative to the wave propagation direction. Each phase, θ_n, of the wave component is set to spatially and temporally focus a theoretical location $x = x_f$ and time $t = t_f$ by

$$\theta_n = -k_n x_f + \omega_n t_f + 2\pi s \quad (s = 0, \pm 1, \pm 2, \ldots). \tag{3}$$

Under a strong opposing current, higher-frequency wave components can be blocked, and no real solution of the

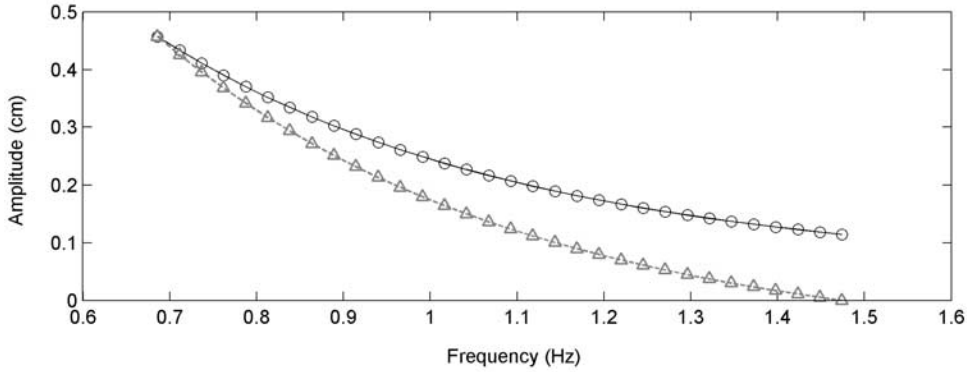

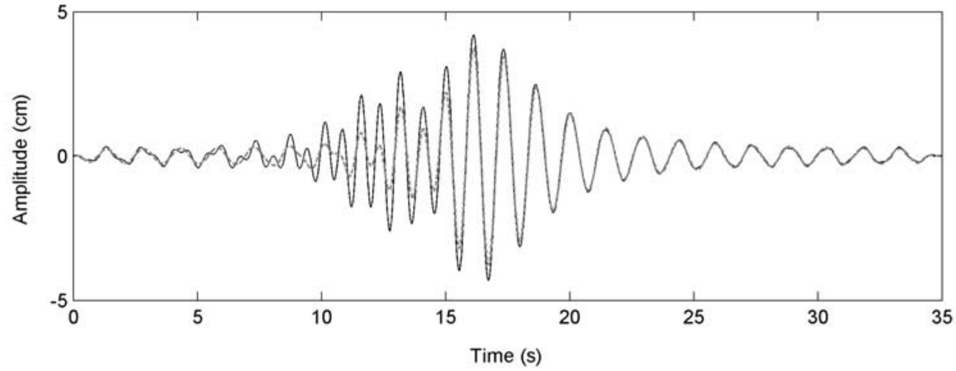

Figure 2. The two input (a) wave amplitude spectra and (b) surface displacements. The symbols, circles with a solid line and diamonds with a dashed line, represent a constant-steepness and linear-steepness spectra, respectively.

wave number can be determined in equation (3) [*Mei*, 1983]. Random phases were assigned for partial wave-blocking cases since a random wave field should not prevent the focusing phenomenon [*Pelinovsky et al.*, 2000; *Slunyaev et al.*, 2002].

[12] The remaining parameter, wave component amplitude a_n, was chosen to represent two different wave spectra at the high-frequency tail. The purpose for this is to examine the effect of wave spectra on limiting freak wave characteristics. In a constant-steepness wave spectrum, amplitude was selected following the inverse of the component wave number [*Baldock et al.*, 1996; *Nepf et al.*, 1998], i.e.,

$$a_n = \frac{G_1}{k_n^0}, \tag{4}$$

where a gain factor, G_1, is used to vary the overall steepness of the wave train, and k_n^0 denotes the wave number corresponding to the apparent frequency ω_n with the superscript of a zero current. In a linear-steepness wave spectrum, amplitude was chosen as

$$a_n = \frac{k_N^0 - k_n^0}{k_n^0\left(k_N^0 - k_1^0\right)} G_2, \tag{5}$$

where G_2 is a gain factor, achieving a linear slope ($a_n k_n^0$) spectrum. By varying the gain factor in equations (4) and (5), different strengths of wave, named as incipient, spilling and plunging waves [*Rapp and Melville*, 1990; *Yao and Wu*, 2004], could be generated. In this study, only incipient (limiting or largest) freak waves without breaking are considered. Figure 2a shows the two input amplitude spectra. A linear-steepness wave spectrum using equation (5) has a steeper or faster-decaying slope than a constant-wave steepness spectrum using equation (4). Other wave spectral distributions, for example, a constant-amplitude spectrum [*Rapp and Melville*, 1990] and the Pierson-Moskowitz spectrum [*Kway et al.*, 1998], have also been used to generate extreme waves.

[13] Substituting equations (2), (3), and (4) or (5) into equation (1) and imposing $x = 0$ gives the surface displacement at the paddle position, i.e.,

$$\eta(x = 0, t) = \sum_{n=1}^{N} a_n \cos(-\omega_n t + \theta_n). \tag{6}$$

Figure 2b shows the designed surface displacements of the two spectra. A faster-growing group envelope is seen in a wave train of linear steepness spectrum, suggesting that any tapering envelop of wave trains can directly affect wave spectra shape and result in a different limiting freak wave. Figures 3a and 3b are photo images of the limiting freak waves on a 10-cm and −10-cm current, respectively. Owing to the Doppler shift effect, the wavelength of the limiting freak wave on opposing currents was shorter than the one on following currents.

[14] Table 1 lists all experimental cases. The capital letters, W and C, indicate wave and current. The effects of spectral slope and spectrum frequency bandwidth on freak wave formation are examined in W1 to W7. For the effects

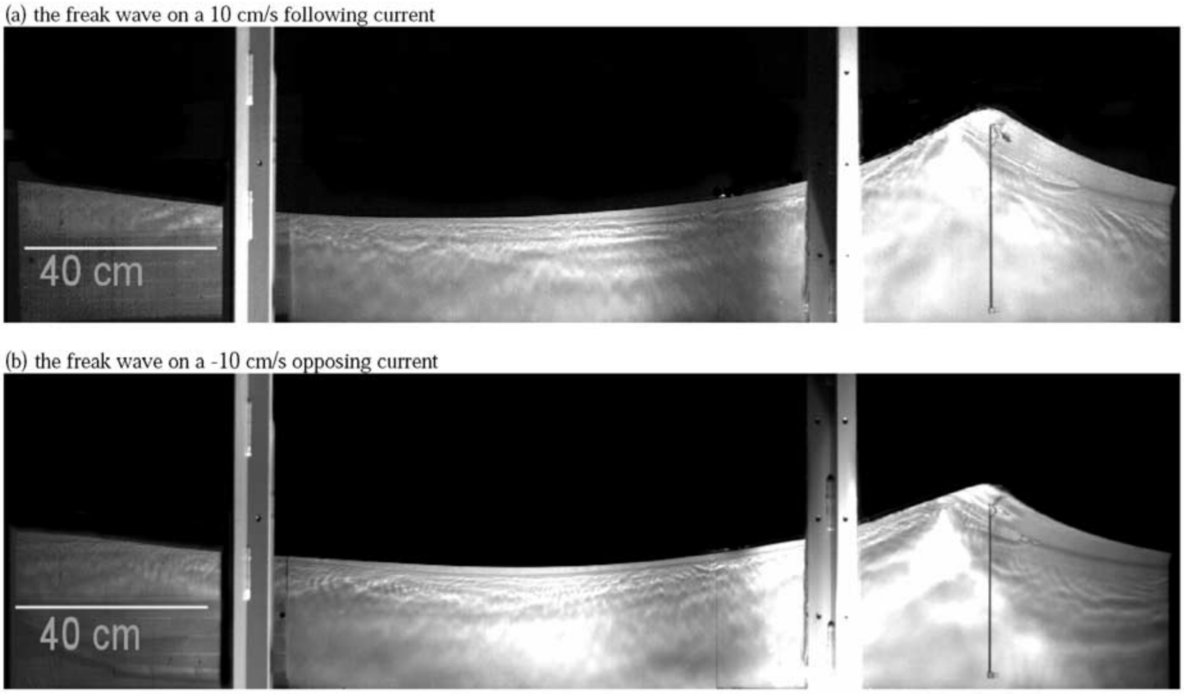

Figure 3. Photograph of the freak wave on (a) a 10 cm/s following current and (b) a −10 cm/s opposing current.

of currents on freak waves, WC1 to WC6 are examined, maintaining the same input wave spectrum, slope, and frequency bandwidth ratio, $\Delta f/f_c$, but varying strengths and directions of current U. Specifically, WC4 to WC6 are the freak waves under partial wave-blocking conditions whose frequency bandwidth ratios were reduced. This kind of freak wave is compared to freak waves with narrow spectral bandwidth without currents (W2 W5, W6, and W7).

3. Data Analysis

3.1. Spectral Bandwidth

[15] Frequency bandwidth and spectral slope of wave groups are important to surface wave characteristics. For example, frequency bandwidth ratio, $\Delta f/f_c$, was shown to affect nonlinear wave group evolutions [*Baldock et al.*, 1996; *Brown and Jensen*, 2001]. In addition, spectral slope is also critical to the formation of extreme waves [*Onorato et al.*, 2001]. To characterize the effects from both frequency bandwidth and spectral slope, we use a nondimensional spectral bandwidth parameter [*Longuet-Higgins*, 1984]

$$\nu = \sqrt{m_2 m_0 / m_1^2 - 1}, \tag{7}$$

where m_i is the ith spectral moment,

$$m_i = \int_0^\infty \omega^i S(\omega) d\omega. \tag{8}$$

To numerically evaluate ν, a band-pass filter with upper and lower cutoffs at $1.5f_p$ and $0.5f_p$ is used, where f_p is the peak spectral frequency. Table 1 gives the designed input spectral bandwidth.

3.2. Geometric Profile

[16] To obtain the largest wave crest steepness of freak waves, a zero-down crossing method was applied to the recorded time series of surface displacements. Two parameters were used to characterize the geometric profiles of freak waves. First, local wave steepness is defined as

$$ak = \frac{H}{2}k, \tag{9}$$

where a, H, and k are local wave amplitude, wave height, and wave number, respectively. The local steepness can be

Table 1. Experimental Cases

Case ID	Current Velocity U, cm/s	Input Wave Spectral Form: Steepness $a_n k_n$	Wave Frequency f_n, Hz	Frequency Bandwidth $\Delta f/f_c$	Spectral Bandwidth ν
W1	0	constant	0.69 ∼ 1.47	0.73	0.195
W2	0	constant	0.69 ∼ 1.10	0.46	0.129
W3	0	constant	0.97 ∼ 1.19	0.2	0.054
W4	0	linear	0.69 ∼ 1.47	0.73	0.154
W5	0	linear	0.69 ∼ 1.10	0.46	0.099
W6	0	linear	0.97 ∼ 1.19	0.20	0.041
W7	0	linear	1.02 ∼ 1.14	0.1	0.021
WC1	10	constant	0.69 ∼ 1.47	0.73	0.195
WC2	10	linear	0.69 ∼ 1.47	0.73	0.154
WC3	−10	linear	0.69 ∼ 1.47	0.73	0.154
WC4	−30	linear	0.69 ∼ 1.47	0.62[a]	0.151
WC5	−35	linear	0.69 ∼ 1.47	0.46[a]	0.124
WC6	−35	linear	0.99 ∼ 2.13	0.1[a]	0.027

[a]Reduction of frequency bandwidth due to partial wave-blocking is estimated using the kinematic conservation equation [*Mei*, 1983].

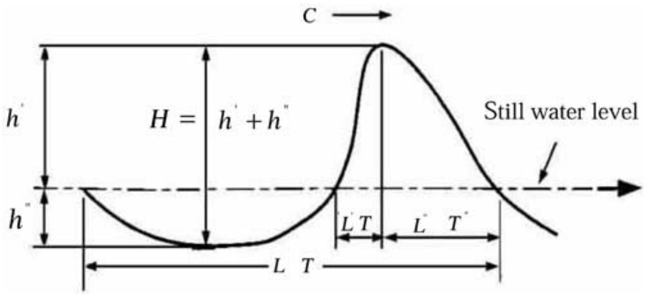

Figure 4. Definition of waveshape parameters by *Myrhaug and Kjeldsen* [1986]. The front-and-rear asymmetry factor $\lambda = \frac{L''}{L'} = \frac{T''}{T'}$ and the up-and-down asymmetry factor $\mu = \frac{h'}{H}$ are used to assess the asymmetry of wave profile. The symbols, *h, L*, and *T,* represent wave height, wavelength, and wave period, respectively.

converted to H/L with $L = {}^{2\pi}/_{k}$, the wavelength. Second, the front-and-rear asymmetry factor $\lambda = {}^{L''}/_{L'} = {}^{T''}/_{T}$ and the up-and-down asymmetry factor $\mu = {}^{h'}/_{H}$, defined in Figure 4, were used to characterize the asymmetrical properties of steep wave profiles [*Myrhaug and Kjeldsen*, 1986]. These two parameters measure the degree of wave asymmetry. All these parameters have been widely used in characterizing profiles of ocean waves in both the laboratory and field [*Sand et al.*, 1990; *Yasuda and Mori*, 1997; *Bonmarin*, 1989; *Griffin et al.*, 1996; *Nepf et al.*, 1998; *Stansell et al.*, 2003; *Soares et al.*, 2004].

[17] To calculate wave number or wavelength using time series of surface displacement, a third-order Doppler-shift dispersion relation,

$$\omega = \sqrt{\left[1 + (ak)^2\left(\frac{8 + \cosh 4kd - 2\tanh^2 kd}{8\sinh^4 kd}\right)\right]kg\tanh(kd)} + kU_c, \tag{10}$$

was used in this study. The capability of a third-order dispersion relation in determining the wave number at steep and breaking waves on opposing currents has been demonstrated [*Chawla and Kirby*, 2002]. Specifically, the third-order dispersion relation takes into account amplitude dispersion up to the order of $O(ak)^2$, which can differ the wave steepness up to 15% using the linear dispersion relation of equation (2). From backlighted image measurements, we found that, in general, the ak calculated by the third-order dispersion relation can be calculated up to 95% accuracy. Therefore the third-order dispersion relation is used for our wavelength estimate.

3.3. Fourier Transformation

[18] Spectral variation is a useful tool in revealing the time history of surface displacement evolution of a wave train in the frequency domain. The Fourier transformation (FT) provides a good tool for resolving frequency spectral evolution of a wave packet along the wave propagation direction. A number of previous studies have employed spectral analysis to examine the dynamics of wave-wave interactions of nonlinear wave packets [*Rapp and Melville*, 1990; *Baldock et al.*, 1996; *Nepf et al.*, 1998; *Johannessen and Swan*, 2001; *Brown and Jensen*, 2001]. In this study, wave energy density spectra were estimated from the time series of surface displacements at all measured locations using the Fast Fourier transform with 14,000 points and a three-point moving-average filter. The total sampling time was 70 s, giving a frequency resolution of 0.014 Hz.

3.4. Hilbert-Huang Transformation

[19] Freak waves are transient and fast-deforming. A nonstationary time-frequency data analysis for resolving temporal and frequency variations of freak waves is desired. To date, several time-frequency spectral analysis techniques [*Liu and Miller*, 1996; *Chien et al.*, 2002; *Mori et al.*, 2002; *Schlurmann*, 2002] have been used. Among them, the Hilbert-Huang Transformation (HHT) method [*Huang et al.*, 1998] has been widely used in analyzing nonstationary and nonlinear time series data in the disciplines of biology, acoustics, and seismology. In recent years, the HHT method has also been applied to oceanography and water waves [*Huang et al.*, 1999; *Schlurmann*, 2002; *Veltcheva*, 2002; *Hwang et al.*, 2003]. Unlike the wavelet time-frequency spectral method, which provides a broad frequency band around the main frequency due to the uncertainty principle [*Cohen*, 1995], the HHT has the capability for clearly delineating the intrawave frequency modulation of monochromatic waves [*Huang et al.*, 1999]. In this paper, we adopted the HHT in examining the evolution of freak waves. A brief introduction to this technique is provided as follows. For further details on the HHT method, the readers can refer to the original literatures [*Huang et al.*, 1998, 1999].

[20] In performing the HHT, a two-step procedure is needed. First, the so-called empirical mode decomposition (EMD) is used to disintegrate time series data into a finite number of local characteristic oscillations. Each oscillation is defined as an "intrinsic mode function" (IMF), meeting two criteria: (1) The number of extrema and the number of zero-crossings must either equal, or differ at most by 1, for the whole data set; and (2) the mean value of the envelope defined by the local maxima and the envelope defined by the local minima is zero at any point. By meeting these two criteria, a series of adaptive sifting processes can be applied to decompose the measured surface displacement time series,

$$\eta(x,t) = \sum_{j=1}^{J}\eta_j(x,t) + r_j(x,t), \tag{11}$$

into different timescales of distinct IMF $\eta_j(x, t)$ components and monotonically varying residue $r_j(x, t)$. The traditional Hilbert transformation is then employed on each $\eta_j(x, t)$ component to determine the instantaneous frequency and instantaneous amplitude.

[21] An analytic signal is defined as

$$Z_j(x,t) \equiv \eta_j(x,t) + i\zeta_j(x,t) = A_j(t)e^{i\phi_j(t)}, \tag{12}$$

where $\zeta_j(x, t)$ is the conjugate of each IMF $\eta_j(x, t)$ and can be obtained through the traditional Hilbert transformation as

$$\zeta_j(x,t) = \frac{P}{\pi}\int_{-\infty}^{+\infty}\frac{\eta_j(x,t)}{\tau - t}d\tau, \tag{13}$$

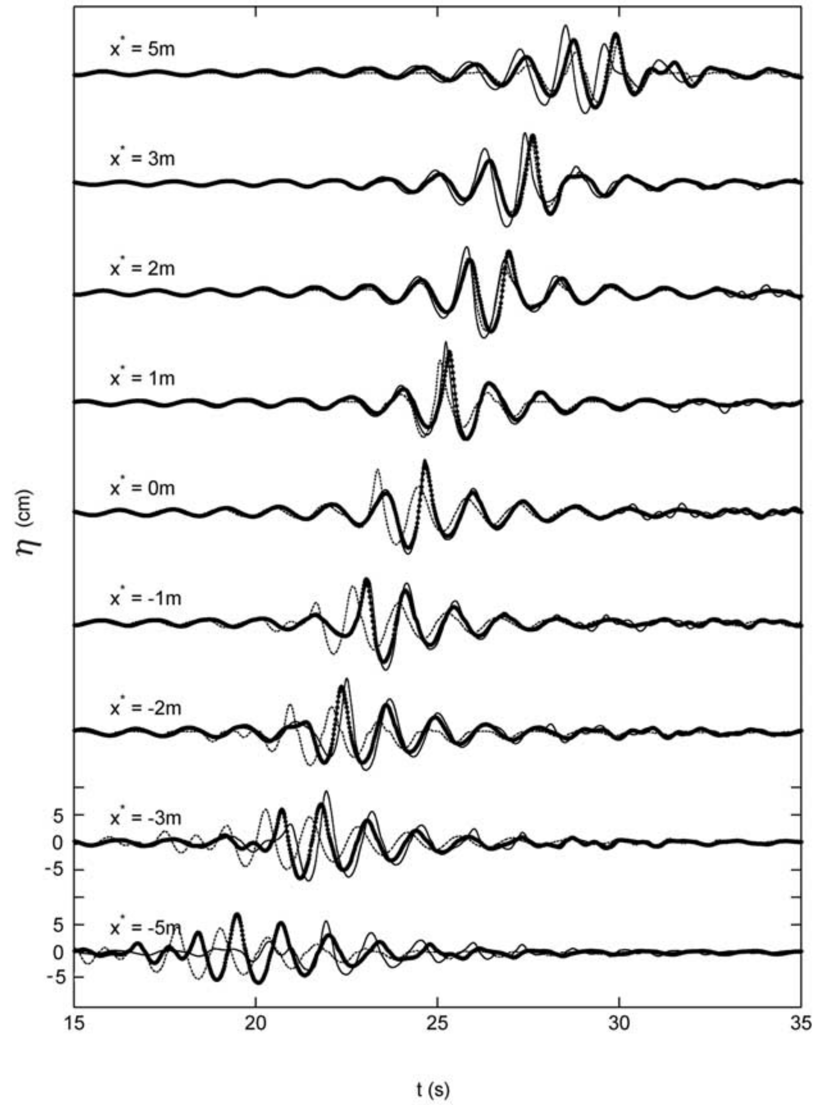

Figure 5. Surface displacement evolution of freak waves on currents of 10 cm/s (solid lines, WC2), 0 cm/s (solid lines with circles, W4), and −10 cm/s (dashed lines, WC3).

with P representing the Cauchy principle value;

$$A_j(x,t) = \sqrt{\eta_j^2(x,t) + \zeta_j^2(x,t)} \tag{14}$$

$$\phi_j(x,t) = \tan^{-1}\left[{}^{\zeta_j(x,t)}/_{\eta_j(x,t)}\right] \tag{15}$$

are the local wave amplitude and local phase, respectively. The local instantaneous frequency is thus defined as

$$f_j(x,t) = \frac{1}{2\pi}\frac{\partial\phi_j(x,t)}{\partial t}. \tag{16}$$

Combining equations (14), (15), and (16), the original wave data are represented by

$$\eta(x,t) = \sum_{j=1}^{J} A_j(x,t)e^{i\int 2\pi f_j(t)dt}, \tag{17}$$

which is analogous to the Fourier transformation representation. Contradictory to the stationary amplitude and frequency sinusoids of the FT method, the HHT allows for a time-varying amplitude and frequency to characterize nonstationary time series features. This time-frequency distribution of the amplitude for each IMF $\eta_j(x, t)$ is designated as the Hilbert spectrum, $H_j(f, t)$ [*Huang et al.*, 1998].

4. Results

4.1. Surface Displacement Evolution

[22] Figure 5 depicts the spatial evolution of the maximum wave trains without breaking on the different currents: zero (W4), 0.1 m/s (WC2), and −0.1 m/s (WC3). Three main features are observed here. First, the wave trains traveled from the upstream (bottom) to the downstream (top). During the focusing process, the frequency dispersive characteristic with the contraction of wave trains due to the longer waves catching up with the shorter waves was clearly

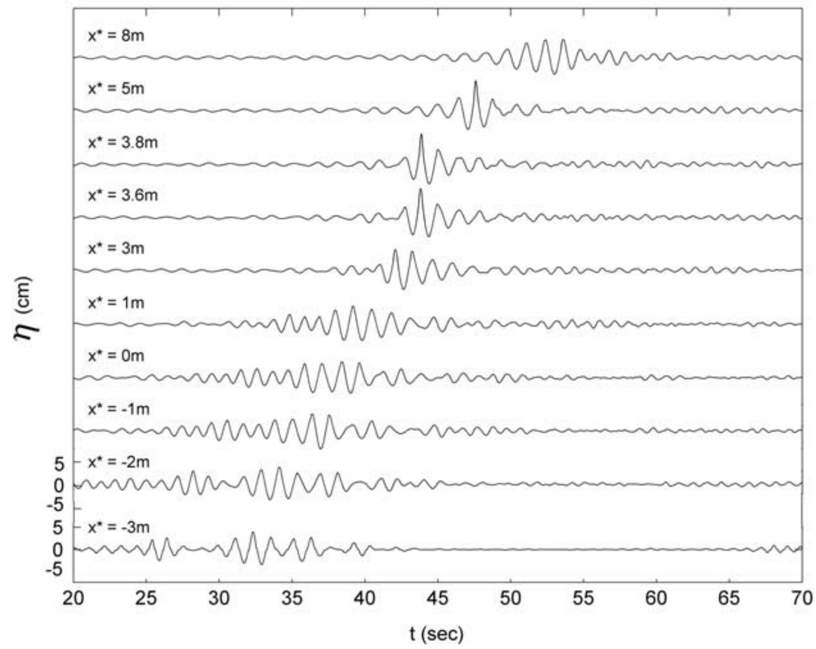

Figure 6. Same as in Figure 5 but for a -35 cm/s strong opposing current (WC6).

seen. While wave trains were designed to spatially focus at $x^* = x - x_{\mathrm{f}} = 0$ (the distance relative to the theoretical focusing point), the observed actual focusing points occurred around $x^* = 1$ m, i.e., downstream of the theoretical focusing points. Indeed, the downstream shifting of the focusing points is more pronounced for freak waves with narrowband or linear-slope spectral than those of broadband or constant-slope spectral, which is believed to be associated with the nonlinearity of wave trains [*Baldock et al.*, 1996]. Second, due to wave-current interactions, the release of the wave packet on the following current was lagged behind the wave packet on zero current; this feature was reversed for the wave packet on the opposing current. The phase arrangement prescribed by the Doppler-shifted dispersion relation in equation (2) ensures that the three wave trains on different strengths of currents focus at the same spatial position. Third, the defocusing process took place after the largest wave crest of each wave train. The three wave trains started to be out of phase with the one on following current leading, followed by the wave train on the zero current, and finally the one on the opposing current. Overall, the above results suggest success on the inclusion of current modulation effects on dispersive freak wave generation.

[23] For waves propagating on strong opposing currents, partial frequency blocking can occur [*Lai et al.*, 1989; *Chawla and Kirby*, 2002]. Figure 6 shows the evolution of the wave train on a -35 cm/s strong opposing current (WC6). The higher-frequency components with assigned random phases in the wave generation clearly appeared in the surface displacements before the focusing location. After that, the strong opposing current acted like a low-pass filter, blocking higher-frequency waves [*Jonsson*, 1990]. The remaining, unblocked lower frequency waves underwent the dispersive process and focused at $x^* \approx 3.8$ m, confirming that random phase wave fields would not prevent focusing phenomena [*Pelinovsky et al.*, 2000; *Slunyaev et al.*, 2002]. However, the observed actual focusing position occurred farther downstream, which may result from the increased nonlinearity for a narrower frequency bandwidth wave train [*Baldock et al.*, 1996; *Brown*, 2001]. Results suggest that nonlinearity plays an important role in determining the location of freak waves. The local geometry of freak waves of different spectral forms in the presence and absence of currents is examined next.

4.2. Geometrical Profile of Limiting Freak Waves

[24] The maximum local wave steepness, *ak*, of limiting freak waves for the experimental cases in Table 1 were calculated using equation (9). Figure 7a plots *ak* versus the frequency bandwidth ratio. As bandwidths of focusing wave packets become narrower (i.e., smaller $\Delta f/f_c$), the limiting wave steepness becomes greater until it reaches $ak = 0.44$ for the deep-water limiting stokes wave. *Alber* [1978] suggested that under the condition of $\Delta f/f_c \leq ak$, the Benjamin-Feir (B-F) instability is able to act on a unidirectional wave train in a limited duration. *Brown and Jensen* [2001] experimentally confirmed that nonlinear effects of the B-F instability can act over a limited duration in focusing narrow bandwidth wave trains, suggesting that $\Delta f/f_c$ indeed is critical to exhibit nonlinear effects. In our experiments, Figure 7a shows the effect of weak following ("plus" symbols) and opposing ("multiplication" symbols) currents on the limiting freak wave profile. The measured *ak* of the limiting freak wave on weak currents remained very close to those without currents, consistent with the observations [*Bonmarin et al.*, 1995] for limiting regular monochromatic wave conditions on weak opposing currents. In contrast, the limiting *ak* (solid circles) was elevated for strong opposing currents which block partial higher frequency waves and reduce the bandwidth of wave trains. This is seen particularly in WC6 with the limiting *ak* remarkably up to 0.36. These results indicate that $\Delta f/f_c$

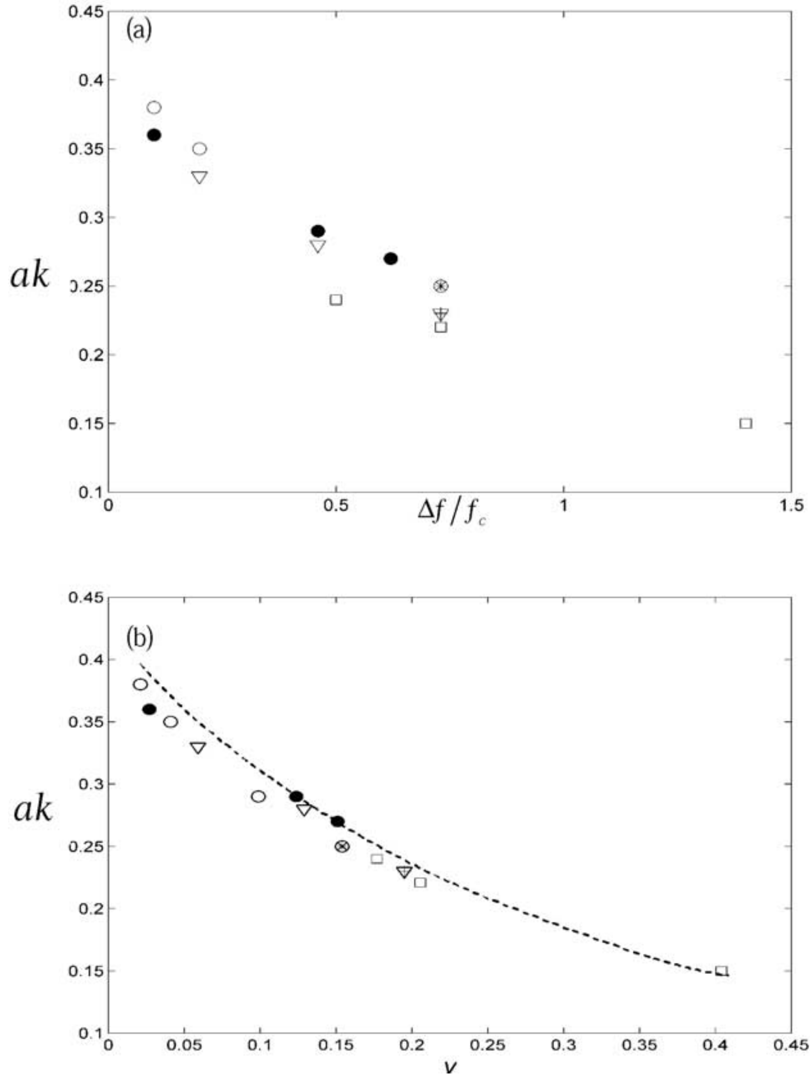

Figure 7. Local wave steepness, *ak*, of limiting freak waves versus (a) frequency bandwidth ratio, $\Delta f/f_c$, and (b) spectral bandwidth, *v*. The symbols, circles, triangles, and squares, represent wave groups of linear-steepness, constant-steepness, and constant-amplitude spectra, respectively. Inside the symbols, the plus, cross, and dot denote following current, weak opposing current, and strong opposing current with partial wave-blocking cases, respectively. The dashed line is the regression curve, $ak = 0.44e^{3.0\nu^2-3.9\nu}$, with $R^2 = 0.97$.

plays a significant role in determining the limiting nonlinear characteristics of freak waves.

[25] In Figure 7a, the effect of different spectral shapes on limiting wave freak wave characteristics is also examined. Three spectral shapes with the same $\Delta f/f_c = 0.73$, circles for the linear-steepness wave spectrum (a_nk_n = linear, W4–W7), triangles for the constant-steepness wave spectrum (a_nk_n = constant, W1–W3), and squares for the constant-amplitude steepness spectrum conducted by *Rapp and Melville* [1990], are compared. It was found that wave groups with a steeper slope spectrum, i.e., the linear slope spectrum, have larger limiting waves, indicating that spectral slopes of dispersive focusing wave groups can significantly change limiting freak waves. Interestingly, recent studies [*Onorato et al.*, 2001; *Mori and Yasuda*, 2002] suggest that freak waves, arisen from the self-focusing B-F instability, are more likely to occur in random wave groups whose spectrum are narrowband by a larger enhancement factor γ and the Phillips constant α [*Komen et al.*, 1994], corresponding to an indeed steeper spectral slope. Thus, spectral slopes of wave groups inherently affect the formation of freak waves due to dispersive frequency focusing or self-focusing B-F instability. Wave groups with a linear steepness wave spectrum usually lead to larger waves without breaking. In other words, a giant, steeper, freak wave is more likely formed in a narrower focused wave train and a steeper slope spectrum.

[26] Combining the effects of frequency bandwidth ratio, $\Delta f/f_c$, and spectral slope, Figure 7b plots the limiting *ak* versus the nondimensional spectral bandwidth parameter *v* with our experiments and those of others [*Rapp and Melville*, 1990] using equations (7) and (8). An excellent correlation between the limiting *ak* and *v* can be seen. This result supports the observations [*Ochi and Tasi*, 1983; *Tulin*

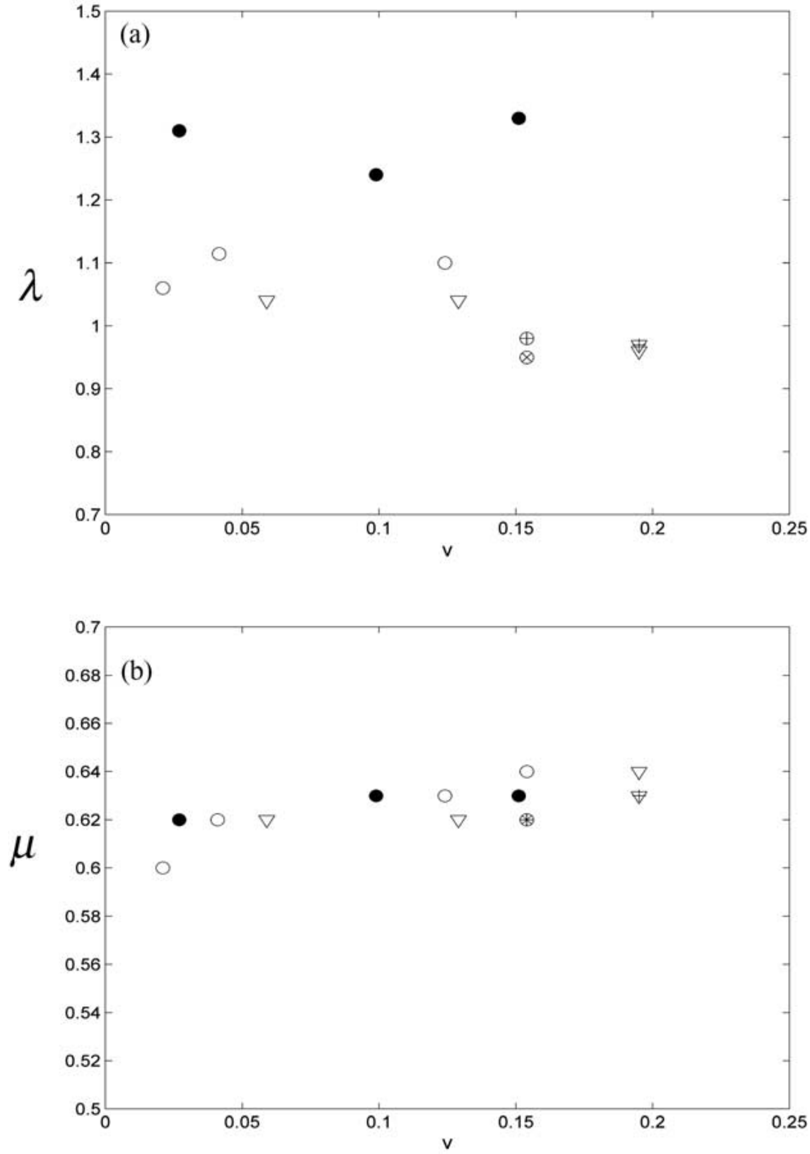

Figure 8. Asymmetry of the limiting wave crest: (a) front-and-rear asymmetry, λ, and (b) up-and-down asymmetry, μ, versus the spectral bandwidth, v. Representations of symbols are the same as in Figure 7.

and Li, 1992] that the wave steepness of ocean waves with a broad distribution of energy in frequency is much lower than that of the Stokes limiting wave, ak = 0.44. Furthermore, this result also provides an explanation that background oceanic turbulence, i.e., broadening the spectrum or an increase of v, may lower breaking criteria in the field relative to the values predicted by theory or observed in pristine tanks [*Wu and Nepf*, 2002; *Kolaini and Tulin*, 1995]. Of importance, the result found here suggests that the spectral bandwidth parameter v of a wave group may serve as a critical parameter in determining the limiting freak wave characteristics, which can affect the occurrence statistics of extreme or freak waves. To the best of our knowledge, the relationship between the maximum ak and v of wave groups has not been revealed before.

[27] To examine asymmetrical characteristics of the limiting wave profile, we plot the front-and-rear asymmetry factor λ and up-and-down asymmetry factor μ versus the spectral bandwidth v in Figures 8a and 8b. One can see that λ is very close to 1, suggesting that λ is not sensitive to v under weak current conditions, consistent with observations in the field [*Myrhaug and Kjeldsen*, 1986]. However, the solid circles (WC4, WC5 and WC6) in Figure 8a show that λ was highly elevated (the freak wave became very asymmetric) when partial higher frequency waves were blocked by strong opposing currents. This feature supports the described asymmetrical profile of freak waves resulting from the wave-current interaction mechanism (e.g., Agulhas Currents [*Mallory*, 1974]). For the up-and-down crest asymmetry, it was found that μ remained fairly constant through all experimental cases, regardless of the different wave spectrum slopes and spectrum bandwidths. The up-and-down asymmetry factor in our tests was around μ = 0.62 $\sim$ 0.64, consistent with field observations, for example, μ = 0.63 in the North Sea [*Myrhaug and Kjeldsen*, 1986] and μ = 0.65 in the Japanese sea [*Mori et al.*, 2002].

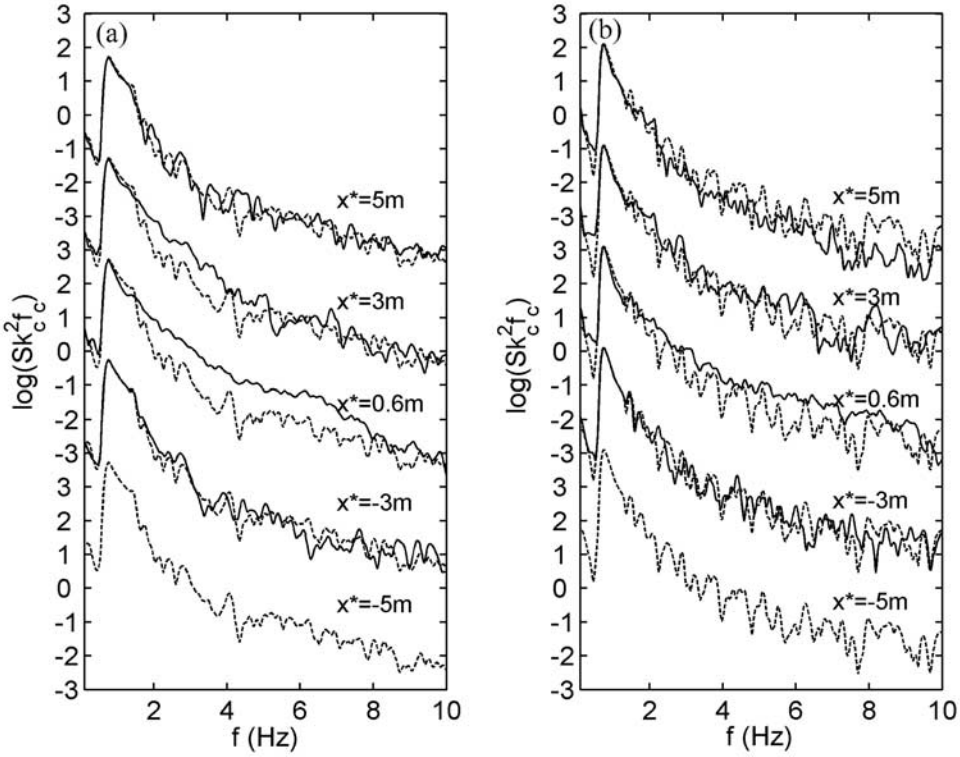

Figure 9. Spatial spectral evolution of the freak wave with (a) a constant-steepness spectrum WC1 and (b) linear-steepness spectrum WC2.

In general, both asymmetry parameters of limiting freak waves generated in the laboratory are in good agreement with reported field observations.

4.3. Spatial Spectral Evolution Using Fourier Spectrum

[28] Figure 9 reveals the spectral energy evolution during the spatial-temporal frequency dispersive-focusing process of freak waves on currents (WC1 and WC2). Wave energy density, S, is normalized by f_c and the input central wave number, k_c. A total of five representative positions, i.e., the two upstream, the actual focal position of the largest wave crest, and the two downstream, is shown here. In the plot, the dash lines and solid lines represent the density spectrum at the upstream reference position and at the marked positions, respectively. During the focusing process, wave-wave interactions became pronounced in the vicinity of $x^* = 0.6$ m. The spectral energy transfer from the input frequency components to higher frequencies is clearly seen, consistent with earlier experimental observations on extreme waves in the absence of currents [*Rapp and Melville*, 1990; *Baldock et al.*, 1996; *Nepf et al.*, 1998; *Brown and Jensen*, 2001]. After the focusing location, wave energy was recovered from the higher frequencies to the input frequency range at $x^* = 5$ m, suggesting that nonlinear energy transfer is reversible. We further examined the effect of spectral slope on freak waves in Figures 9a and 9b. At the focusing location $x^* = 0.6$ m, there was a distinguished signature of energy density spectrum at the higher frequencies. This energy transfer to the higher frequency was less significant for WC2 with the linear slope spectrum than for WC1 with the constant slope wave spectrum, suggesting that spectral slope may control the degree of energy transfer to higher frequency during the occurrence of freak waves.

[29] To examine the effect of a strong opposing current (WC5) interacting with freak waves, Figure 10a shows the spectral evolution at five representative spatial positions. At $x^* = -5$ m, a good matching of the measured spectra and the input spectrum (open circles) indicates the success in our wave energy generation. At $x^* = -2$ m the wave energy slightly greater than the frequency $f \approx 1.1$ Hz was blocked, consistent with the theoretical estimate using the kinematic conservation equation [*Mei*, 1983] A pile-up of spectral energy just below the blockage frequency was clearly discernible. Similar phenomena of energy pile-ups have been earlier noted [*Huang et al.*, 1972] and later confirmed in the laboratory [*Lai et al.*, 1989; *Chawla and Kirby*, 2002]. Owing to blocking and nonlinear processes, the freak wave did not occur at the designed location until $x^* = 3.8$ m, where energy transfer to higher frequencies was observable. After that, the wave train continuously propagated downstream. At $x^* = 6.0$ m, the spectrum shrank, and a significant amount of wave energy in the high-frequency range disappeared due to the strong opposing current. Furthermore, a slight downshift of the spectral peak was visible, which was absent from the freak waves on weak currents. Similar spectrum evolution patterns with partial wave blocking were observed in the strong opposing currents (WC4 and WC6) but are not shown here for the purpose of brevity. Interestingly, a recent article on examining propagation of a narrow-banded wave train against strong opposing currents (A. Chawla and J. T. Kirby, Propagation of weakly non-linear, narrow-banded waves against strong currents, submitted to *Journal of Fluid*

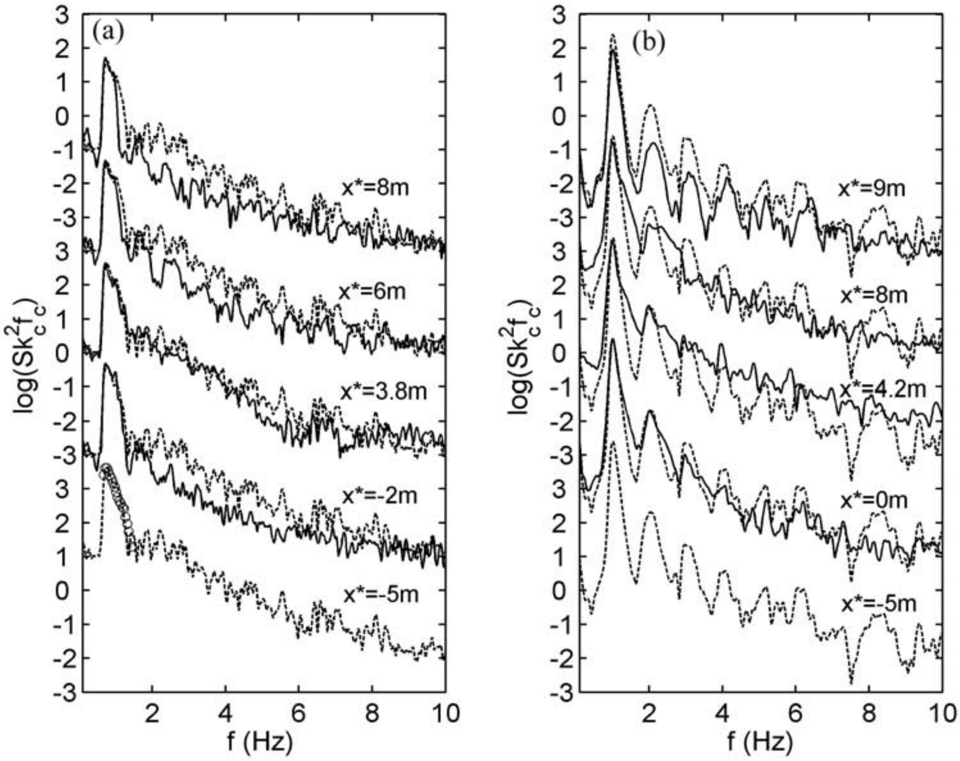

Figure 10. Same as in Figure 9 but for (a) −35 cm/s strong opposing current WC5 and (b) a narrow-banded spectrum W6.

Mechanics, 2004) shows that nonlinear amplitude dispersion effects can considerably delay the blocking location and thus affects the dynamics of the wave field beyond the blocking location. Overall these results indicate that a strong opposing current acting on a propagating wave train reduces $\Delta f/f_c$ or v of the wave train, thus influencing the energy spectrum of freak waves.

[30] The effect of narrow frequency bandwidths on focusing freak waves is examined in Figure 10b. At $x^* = -5$ m, multiple-peaked spectra at the higher frequency tail are seen, which can be interpreted as forced or bound waves. Since the $\Delta f/f_c = 0.2$ is smaller than the wave steepness *ak*, the Benjamin-Feir instability [*Benjamin and Feir*, 1967] is expected to act on a unidirectional deep-water wave train [*Alber*, 1978; *Brown and Jensen*, 2001]. At $x^* = 0$ m, energy from the spectral peak transferred to both the lower- and higher-frequency sidebands. Owing to the nonlinear wave-wave interactions, the freak wave did not occur until $x^* \sim 4.2$ m, where the up-and-down energy transfer (the growth of lower and higher sidebands) was visible and the spectrum was broadening. A recurrence process immediately took place after that. At $x^* = 9$ m, a slight energy drop at the peak was noticed. One reason that the wave spectrum was not at a full recovery at this location may be due to friction from the sidewalls. Another possibility would be that the measured distance was not enough for a full recovery of the wave packet. Regardless of either reason, no downshifting for the narrow-banded focusing wave trains was observed (with a resolution of 0.014 Hz using the FT), consistent with the observations for a discrete three-wave train system [*Tulin and Waseda*, 1999].

[31] Finally, using the FT, we see that the spatial spectral evolution of freak waves from a focusing wave train can be described to a certain extent. The spectral signature of energy transfer to high-frequency waves is a good indicator for the location where a freak wave occurs. However, this spectral signature is less distinct for a higher freak wave with a steeper slope spectrum. In other words, detecting higher, steeper freak waves using the FT becomes more challenging. A different viewpoint for revealing time-frequency energy signatures of freak waves will be addressed next.

4.4. Spatial and Temporal Spectral Evolution Using the HHT

[32] Following the two-step procedure described in section 3.4, Figure 11 presents the original surface displacement and the IMFs with their corresponding phases of the WC1 freak wave using the EMD. Note that the original surface displacement (Figure 11, top panel) was decomposed into eight IMF components. Only the first three IMF components, C_1 to C_3, are shown here since the other five IMF components are at least 2 or 3 orders of magnitude smaller than C_3. These three IMFs have distinct characteristic timescales, demonstrating the capability of intrinsic-oscillation-based features by the EMD. At t = 25.2 s, the focusing phenomenon was clearly exhibited in the first three IMF components. The central wave crest of η_1 neatly lined up with the highest crests in η_2 and η_3 in time (in phase), forming the crest of the freak wave (Figure 11, top panel). In contrast, the two adjacent wave crests next to the largest one of the η_1 IMF were out of phase with those of η_2 and η_3. The arrangement of "in" and "out of" phases for these

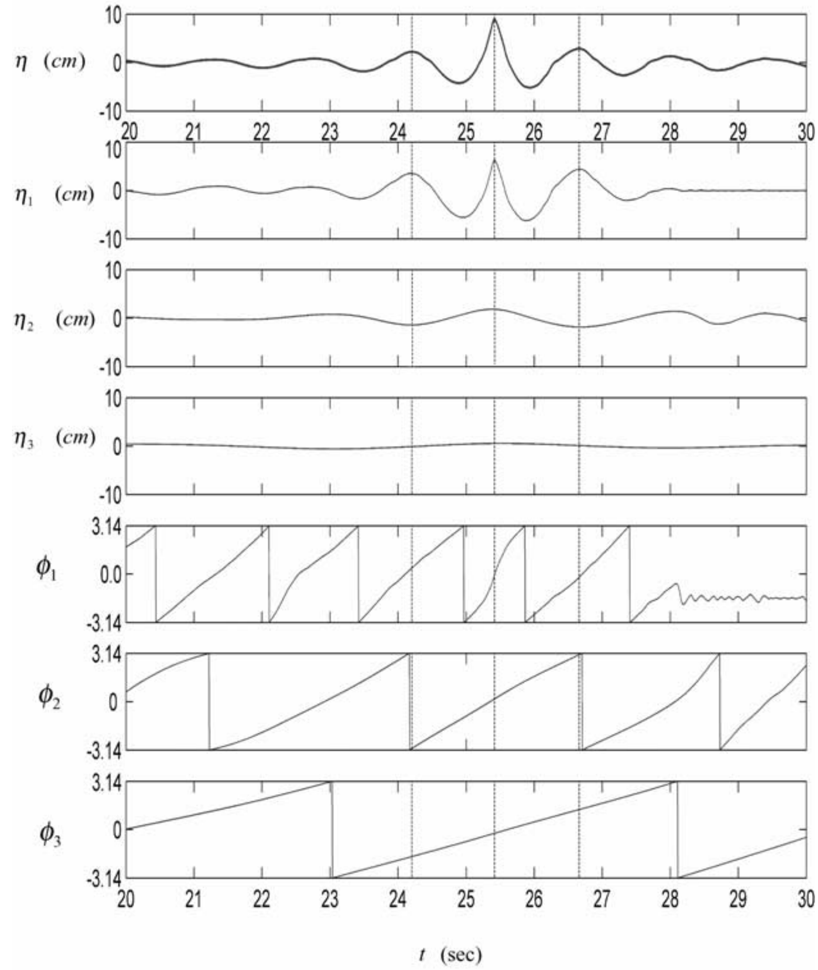

Figure 11. (top panel) Original surface displacement of WC1. (second through fourth panels) IMFs are denoted by η_1, η_2, and η_3, with their associated phases fifth through seventh panels) ϕ_1, ϕ_2, and ϕ_3. The three dashed lines correspond to the main freak wave and its two adjacent wave crests.

IMFs, delineated by the HHT, resulted in a larger crest and a milder trough of the freak wave.

[33] Figure 12 depicts the spatial and temporal evolution of the Hilbert amplitude spectra, $H_1(f, t)$ and $H_2(f, t)$, corresponding to the first two most energetic η_1 and η_2 IMF components of the WC1. (Note that the first two IMF components carry almost 95% of the energy in the wave train.) The label, x^*, on each plot marks the spatial position relative to the theoretical linear focusing location. The axis, $t^* = t - t_f$, denotes the time relative to the theoretical focusing time. The shaded intensity bar beneath the plot denotes the magnitude of the instantaneous frequency (IF) and amplitude, i.e., Hilbert amplitude spectra. In Figure 12a, variations of $H_1(f, t)$ along the spatial position are clearly seen, indicating the nonlinear, transient features of so-called intrawave modulation [*Huang et al.*, 1999]. At $x^* = -5$ m, $H_1(f, t)$ displayed the feature of the high-frequency components leading the low-frequency ones, consistent with the freak wave generation concept that low-frequency long waves are generated later to catch earlier released high-frequency short waves through dispersive frequency focusing. From $x^* = -5$ m to -3 m, the dispersive focusing process took place, resulting in the growth of wave amplitude and nonlinearity in $H_1(f, t)$. At $x^* = 1.2$ m and $t^* = 0.26$ s, a sudden increase of instantaneous frequency in $H_1(f, t)$ up to 2.3 Hz was evident, suggesting that the wave energy was instantaneously transferred to the higher-frequency components. This rapid increase in intrawave modulation indeed coincided with the appearance of the short-lived, largest freak wave. A similar trend for freak waves in the absence of currents has also been reported [*Schlurmann*, 2002]. Following the position of the giant wave, intrawave modulation subsided quickly and a reverse signature of $H_1(f, t)$ at $x^* = 5$ m, in comparison with that at $x^* = -5$ m, was observed. For $H_2(f, t)$, Figure 12b shows the IF maintained at approximately the input central frequency 0.73 Hz before $t^* = 0$. No significant signatures of intrawave modulation were observed, suggesting that $H_2(f, t)$ can be viewed as the carrier frequency. In comparison to the Fourier spectral evolution in Figure 9a that shows the wave energy transfer/redistribution to the higher frequency at $x^* = -0.5$ m, Figure 12 provides additional information on the time-frequency-amplitude evolution of freak waves. Specifically, unlike the Fourier representation, the existence of energy at a frequency means the energy persists over the entire timespan of the data set. The HHT reveals the

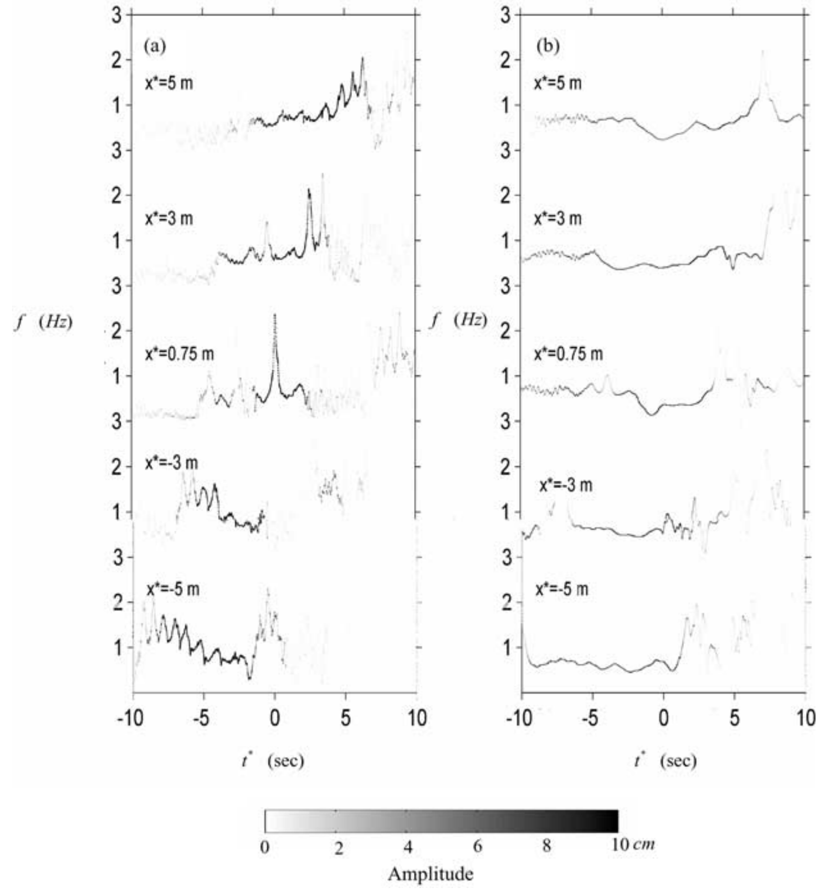

Figure 12. Hilbert spectrum for the freak wave on a 10 cm/s current (WC1). (a) $H_1(f, t)$ and (b) $H_2(f, t)$ for the IMF η_1 and η_2, respectively.

frequency evolution of a strong intrawave modulation at a particular time instant, which matches to the occurrence of freak waves.

[34] Figures 13a and 13b present the spatial and temporal evolution of $H_1(f, t)$ and $H_2(f, t)$ for a freak wave on a strong opposing current (WC5). At $x^* = -5$ m, unlike the freak wave on the following current in the previous case, almost no high-frequency waves and almost zero amplitudes exist in $H_1(f, t)$ since these waves have been blocked. Indeed, the signature for partial wave-blocking at high-frequency components was shown at all measured locations except for the position $x^* = 3.8$ m where the freak wave occurred. At $t^* = 2.2$ s, an abrupt increase of intrawave frequency modulation up to 1.9 Hz appeared in $H_1(f, t)$. Furthermore, there was a redistribution of wave energy to the low-frequency components in $H_2(f, t)$, giving a concave shape between $t^* = 2.2$ s and = 5.0 s. This downshifting energy transfer was retained further downstream at $x^* = 8.0$ m. Previous studies suggest that spectral downshifting can occur in wave blocking with breaking [*Tulin and Waseda*, 1999; *Lai et al.*, 1989; *Chawla and Kirby*, 2002], which is believed to be the cause for permanent downshifting. Nevertheless, Figure 13b shows that partial wave-blocking without breaking redistributed energy to low frequencies so that a permanent frequency downshifting occurred. Further research on the feature of a permanent downshifting due to a partial wave-blocking condition is needed.

[35] Signature of energy transfer to high-frequency waves on the occurrence of freak waves, using the FT, has been identified in section 4.3. However, it is recognized that this signature is less pronounced for higher and steeper freak waves. The HHT provides a mean to re-examine this signature. Let IF_1 and IF_2 denote the instantaneous frequencies for H_1 (intraspectral modulation) and H_2 (carrier wave), respectively. The difference of the instantaneous frequency for H_1 and H_2, i.e., $\Delta F_{12} = IF_2 - IF_1$, at the instant of freak wave occurrence can then serve as an indicator of interwave modulation. In Figures 12 and 13, ΔF_{12} was estimated at about 1.9 Hz and 1.5 Hz for the freak wave on the weak and strong opposing current, respectively. There seems to have a correlation between a smaller interwave frequency and a steeper and asymmetric freak wave (a strong opposing current or smaller spectral bandwidth). In other words, a difference amount in interwave frequency appears to be reflected in the nondimensional spectral bandwidth parameter ν.

[36] To further assess the above feature, Figure 14 displays the H_1 and H_2 for six freak waves with different spectrum slopes or frequency bandwidths. In Figures 14a and 14b, ΔF_{12} of the freak waves was approximately 1.9 Hz (W1: constant-steepness spectrum) and 1.7 Hz (W4: linear-steepness spectrum), respectively. A smaller ΔF_{12} corresponds to a freak wave with a steeper spectral slope. To examine the effect of frequency bandwidth,

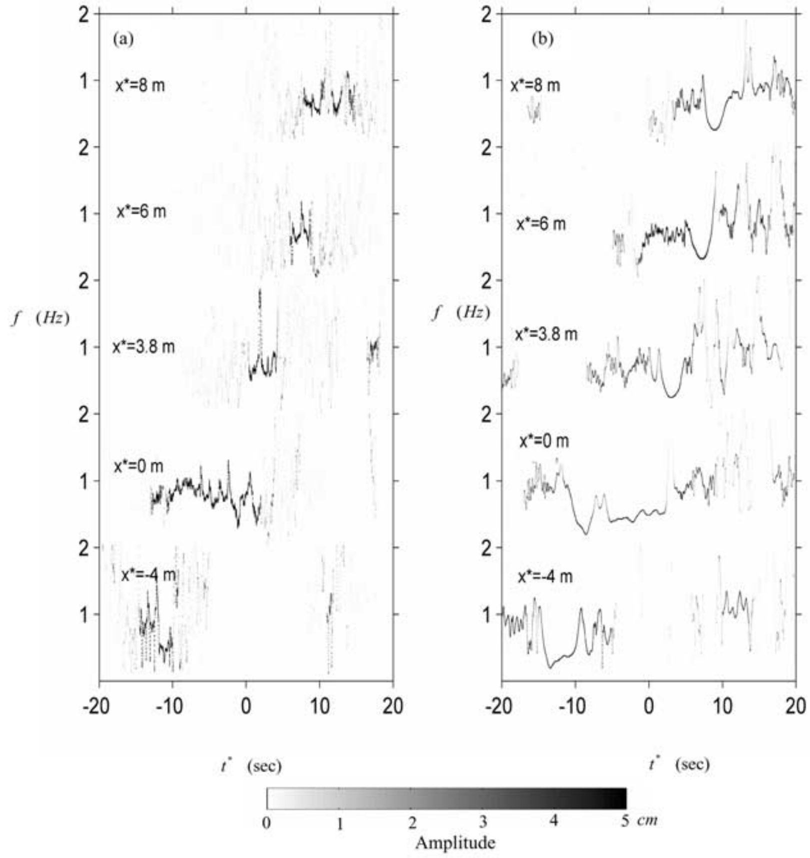

Figure 13. Same as in Figure 12 but for the freak wave on a −35 strong opposing current (WC5).

ΔF_{12} in Figure 14d was 1.6 Hz (W4: linear steepness spectrum with a smaller frequency bandwidth $\Delta f/f_c = 0.46$), corresponding to a smaller v. Furthermore, ΔF_{12} was found to be approximately 1.7 Hz (WC2: linear steepness spectrum with 10 cm/s current) in Figure 14c. Since the following current did not change the v value in this case, the ΔF_{12} maintained a similar value as the one in Figure 14b. Combining the results here and in Figure 7b shows that ΔF_{12} reflects the range of interwave frequency and determines the limiting wave steepness ak. The smaller ΔF_{12} is, the larger ak of a limiting freak wave is going to be. The unique feature that a smaller ΔF_{12} corresponding to a steeper slope spectrum or a narrower frequency bandwidth results in a steeper or more nonlinear focusing freak wave, for the first time, is revealed in this study.

[37] The Benjamin-Feir instability plays an important role once the bandwidth of deep-water wave group is small [*Benjamin and Feir*, 1967; *Lake et al.*, 1977; *Su et al.*, 1982; *Tulin and Waseda*, 1999]. In addition, the Benjamin-Feir instability acts over a limited duration in a focusing wave group whose bandwidth is narrow [*Brown and Jensen*, 2001; *Alber*, 1978]. Figures 14e and 14f show H_1 and H_2 for the frequency bandwidth $\Delta f/f_c = 0.2$ and 0.1, respectively. As $\Delta f/f_c$ became smaller, H_1 (intrawave frequency modulation) was much more pronounced, in comparison to Figures 14a–14d. Furthermore, the offset of the theoretical occurrence of the freak wave increased, i.e., 2.4 s for Figure 14e and 13.5 s for Figure 14f, suggesting that the nonlinear effect became more important. Specifically, for a very narrow frequency bandwidth ($\Delta f/f_c = 0.1$), the local limiting freak wave steepness is $ak = 0.38$ (see Figure 7a). The evolution time was roughly after 60 central wave periods, which undoubtedly resulted from the Benjamin-Feir sideband instability. This instability may overwhelm intrawave frequency modulation for freak waves resulting from spatial-temporal frequency dispersive focusing. As a result, the feature of larger interwave frequency ΔF_{12} associated with a higher nonlinear freak wave is contradictory to our previous heuristic observation results for freak waves due to dispersive focusing. Future studies are needed to further reveal the feature of ΔF_{12} for freak waves resulting from different mechanisms and take the Hilbert amplitude into consideration in examining wave steepness evolution.

5. Conclusions and Recommendations

[38] Detailed laboratory measurements of freak waves generated through dispersive focusing and wave-current interactions were conducted. A number of factors controlling limiting freak wave characteristics were examined. Experimental findings indicate that wave group structure is critical to the formation of freak waves. Both spectral slope and frequency bandwidth strongly affect the geometric properties of freak waves. Wave groups with steeper spectrum slopes potentially result in steeper freak waves. Furthermore, wave groups with narrower frequency bandwidths exhibit stronger nonlinear and asymmetric freak

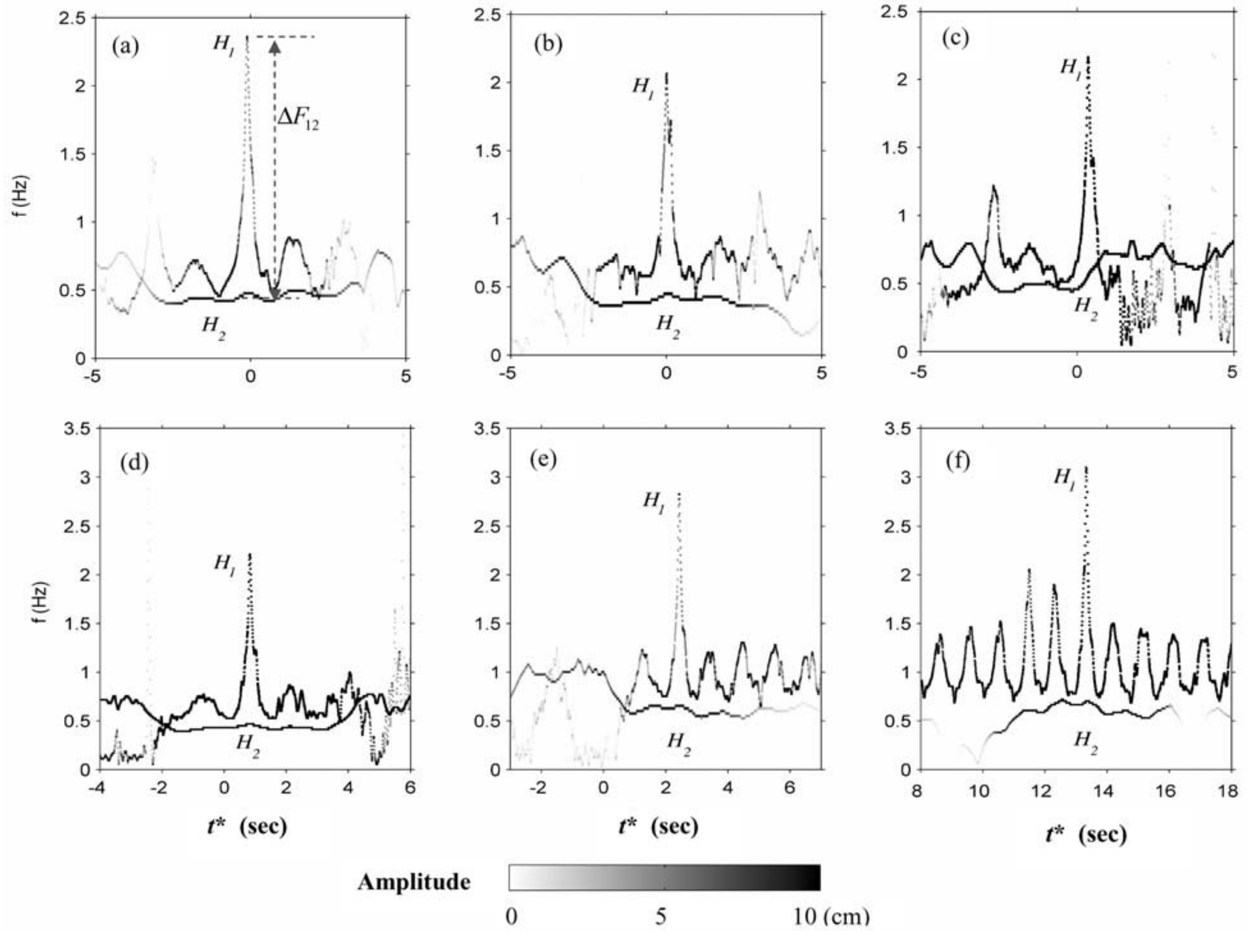

Figure 14. Hilbert spectrum for the freak wave occurring in (a) constant-steepness spectrum W1, (b) linear-steepness spectrum W4, (c) linear-steepness spectrum on a 10 cm/s current WC2, (d) linear-steepness spectrum with $\Delta f/f_c$ = 0.46, W5, (e) linear-steepness spectrum with $\Delta f/f_c$ = 0.20, W6, and (f) linear-steepness spectrum with $\Delta f/f_c$ = 0.10, W7.

wave profiles. A nondimensional spectral bandwidth that represents both the spectral slope and frequency bandwidth behaviors proves to be a good indicator in determining limiting freak wave characteristics, which can affect the occurrence statistics of extreme or freak waves. To the best of our knowledge, the relationship between ν and limiting freak wave characteristics has not been revealed before.

[39] The role of a co-existing current in the formation of freak waves is recognized. While weak opposing currents (no wave-blocking) do not affect the local geometrical steepness of limiting freak waves, strong opposing currents with partial wave-blocking can significantly change the kinematics and dynamics of freak waves. Reduction in frequency bandwidth and downshift of spectral peak of a wave group are observed. This reduction leads to a smaller nondimensional spectral bandwidth, which is well correlated with the elevated limiting steepness (nonbreaking) and asymmetry of freak waves. This laboratory study supports the theoretical explanation of abnormal freak wave formation in a strong opposing current [*Smith*, 1976; *Lavrenov*, 1998]. Moreover, our experiments confirm that a wave random field does not prevent freak wave formation due to dispersive focusing [*Pelinovsky et al.*, 2000; *Slunyaev et al.*, 2002].

[40] The spectral evolution of freak waves in focused wave groups is examined. At the location where a freak wave occurs, the Fourier transformation displays the distinguished feature of energy transfer to high-frequency waves [*Rapp and Melville*, 1990; *Baldock et al.*, 1996; *Nepf et al.*, 1998; *Wu and Nepf*, 2002]. This feature is complicated by the discrimination of bound waves and free waves if a physical interpretation is sought for [*Johannessen and Swan*, 2001; *Huang et al.*, 1999], which is inherently due to the nonlinear nature of freak waves. In this study, we show that the Hilbert-Huang transformation provides an effective tool to examine nonstationary and nonlinear time series data. The time-frequency-amplitude distribution of the Hilbert spectrum vividly depicts temporal and spatial freak wave evolution. In particular, instantaneous frequency modulation yields a more meaningful interpretation for the nonlinearity in freak waves. The difference of the instantaneous frequency, i.e., ΔF_{12}, indicates the magnitude of interwave modulation. Our experiments show that there is a strong correlation between ΔF_{12} and the associated nonlinearity (steepness) of freak waves, which in turn are subject to wave group structure: frequency bandwidth and spectrum slope. This correlation has a different trend, depending on the mechanism of generating freak waves.

For a freak wave evolving from a dispersive-focusing wave group with a relatively broadband and milder spectrum slope, ΔF_{12} decreases with a higher nonlinearity limiting wave. On the other hand, for freak wave occurring in a wave group with a narrowband and steeper spectrum slope, this correlation can be reversed, probably due to the overwhelming Benjamin-Feir instability.

[41] To further understand rare but devastating freak waves in coastal and open oceans, more realistic oceanic conditions should be considered, including for example, three-dimensional waves on random wave background and spatially (vertically or horizontally) sheared currents, wind-forcings, variable bathymetries, etc. The importance of wave directionality of focused wave groups has been highlighted [*Johannessen and Swan*, 2001; *Wu and Nepf*, 2002]; The reduction in directional spreading of three-dimensional wave trains has been shown to be more likely to promote freak waves generated by modulation instability [*Onorato et al.*, 2002]. On the other hand, *Slunyaev et al.* [2002] argued that the geometric-focusing mechanism may play a more important role in three-dimensional wave trains. Surface sheared currents, generated by wind-forcing, can reduce maximum limiting wave height [*Banner and Phillips*, 1974; *Banner and Tian*, 1998]. The effect of wind on the generation of freak waves was recently reported [*Giovanangeli et al.*, 2004]. It was found that a freak wave under a light wind condition maintains its coherency but occurs at a longer fetch. However, a larger-amplitude freak wave under a wind-forcing condition was observed. Further examination of the effects of atmospheric forcing and surface sheared current on freak wave formation and limiting characteristics is highly desired.

[42] **Acknowledgments.** This study was supported by the Wisconsin Alumni Research Foundation, and the College of Engineering at UW-Madison. The authors specifically thank James B. Edson at the Woods Hole Oceanographic Institution for his mentoring support. We also thank Nanette Kelsey for her helpful editorial comments.

References

Alber, I. E. (1978), The effects of randomness on the stability of two-dimensional wavetrains, *Proc. R. Soc. London, Ser. A*, *363*, 525–546.

Baldock, T. E., C. Swan, and P. H. Taylor (1996), A laboratory study of nonlinear surface waves on water, *Philos. Trans. R. Soc. London, Ser. A*, *452*, 649–676.

Banner, M. L., and O. M. Phillips (1974), On the incipient breaking of small scale waves, *J. Fluid Mech.*, *65*, 647–656.

Banner, M. L., and X. Tian (1998), On the determination of the onset of breaking for modulating surface gravity water waves, *J. Fluid Mech.*, *367*, 107–137.

Benjamin, T., and J. Feir (1967), The disintegration of wave trains in deep water, *J. Fluid Mech.*, *27*, 373–397.

Bonmarin, P. (1989), Geometric properties of deep water breaking waves, *J. Fluid Mech.*, *209*, 405–433.

Bonmarin, P., F. Bartholin, and A. Ramamonjiarisoa (1995), Action of an adverse current on the shape of deep-water surface-waves, *Exp. Fluids*, *18*, 438–444.

Brown, M. G. (2001), Space-time surface gravity wave caustics: Structurally stable extreme wave events, *Wave Motions*, *33*, 117–143.

Brown, M. G., and A. Jensen (2001), Experiments on focusing unidirectional water waves, *J. Geophys. Res.*, *106*(C8), 16,917–16,928.

Chawla, A., and J. T. Kirby (2002), Monochromatic and random wave breaking at blocking points, *J. Geophys. Res.*, *107*(C7), 3067, doi:10.1029/2001JC001042.

Chen, H. H., and C. S. Liu (1976), Solitons in nonuniform media, *Phys. Rev. Lett.*, *37*, 693–697.

Chien, H., C. C. Kao, and L. Z. H. Chuang (2002), On the characteristics of observed freak waves, *Coastal Eng. J.*, *44*(4), 301–319.

Cohen, L. (1995), *Time Frequency Analysis*, Prentice Hall, Old Tappan, N. J.

Dean, R. G. (1990), Freak waves: A possible explanation, in *Water Wave Kinematics*, edited by O. Torum and O. T. Gudmestad, pp. 609–612, Kluwer Acad., Norwell, Mass.

Draper, L. (1965), Freak ocean waves, *Mar. Obs.*, *35*, 193–195.

Dysthe, K. B. (2001), Refraction of gravity waves by weak current gradients, *J. Fluid Mech.*, *442*, 157–159.

Dysthe, K. B., and K. Trulsen (1999), Note on breather type solutions of the NLS as a model for freak-waves, *Phys. Scr. T*, *82*, 48–52.

Forristall, G. Z. (1984), The distribution of measured and simulated wave heights as a function of spectral shape, *J. Geophys. Res.*, *89*(C6), 10,547–10,552.

Giovanangeli, J. P., C. Kharif, and E. Pelinovsky (2004), An experimental study on the effect of wind on the generation of freak waves (abstract), paper presented at First General Assembly, Eur. Geosci. Union, Katlenburg-Lindau, Germany.

Glauss, G. (2002), Task related wave groups for seakeeping tests or simulation of design storm waves, *Appl. Ocean Res.*, *24*, 147–161.

Griffin, O. M., R. D. Peltzer, H. T. Wang, and W. W. Schultz (1996), Kinematic and dynamic evolution of deep water breaking waves, *J. Geophys. Res.*, *101*(C7), 16,515–16,531.

Haver, S., and O. J. Andersen (2000), Freak waves: Rare realization of a typical population or typical realization of a rare population?, paper presented at 10th International Offshore Polar Engineering Conference, Int. Soc. of Offshore Polar Eng., Seattle, Wash.

Henderson, K. L., D. H. Peregrine, and J. W. Dold (1999), Unsteady water wave modulations: Fully nonlinear solutions and comparison with the nonlinear Schrödinger equation, *Wave Motion*, *29*, 341–361.

Huang, N. E., D. T. Chen, C. C. Tung, and J. R. Smith (1972), Interactions between steady non-uniform currents and gravity waves with applications for current measurements, *J. Phys. Oceanogr.*, *2*, 420–431.

Huang, N. E., Z. Shen, S. Long, M. C. Wu, H. H. Shih, Q. Zheng, C. C. Tung, and H. H. Liu (1998), The empirical mode decomposition and the Hilbert spectrum for nonlinear and non-stationary time series analysis, *Proc. R. Soc. London, Ser. A*, *454*, 903–995.

Huang, N. E., Z. Shen, and S. Long (1999), A new view of nonlinear water waves: The Hilbert spectrum, *Ann. Rev. Fluid Mech.*, *31*, 417–457.

Hwang, P. A., N. E. Huang, and D. W. Wang (2003), A note on analyzing nonlinear and non-stationary ocean wave data, *Appl. Ocean Res.*, *25*, 187–193.

Janssen, P. A. E. M. (2003), Nonlinear four-wave interactions and freak waves, *J. Phys. Oceanogr.*, *33*, 863–884.

Johannessen, T. B., and C. Swan (2001), A laboratory study of the focusing of transient and directionally spread surface water waves, *Philos. Trans. R. Soc. London, Ser. A*, *457*, 971–1006.

Jonsson, I. G. (1990), Wave current interactions, in *The Sea*, *Ocean Eng. Sci.*, vol. 9a, pp. 65–120, John Wiley, Hoboken, N. J.

Kharif, C., and E. Pelinovsky (2003), Physical mechanisms of the rogue wave phenomenon, *Eur. J. Mech. B Fluids*, *22*, 603–634.

Kharif, C., E. Pelinovsky, T. Talipova, and A. Slunyaev (2001), Focusing of nonlinear wave groups in deep water, *JETP Lett.*, *73*, 170–175.

Kjeldsen, S. P. (1984), Dangerous wave groups, *Nor. Mar. Res.*, *12*, 453–473.

Kjeldsen, S. P. (1990), Breaking waves, in *Water Wave Kinematics*, edited by O. Torumand and O. T. Gudmestad, pp. 453–473, Kluwer Acad., Norwell, Mass.

Kolaini, A., and M. P. Tulin (1995), Laboratory measurements of breaking inception and postbreaking dynamics of steep short-crested waves, *Int. J. Offshore Polar Eng.*, *5*, 212–218.

Komen, G. J., L. Cavaleri, M. Donelan, K. Hasselmann, S. Hasselmann, and P. A. E. M. Janssen (1994), *Dynamics and Modeling of Ocean Waves*, Cambridge Univ. Press, New York.

Kway, J. H. L., Y. S. Loh, and E. S. Chan (1998), Laboratory study of deep-water breaking waves, *Ocean Eng.*, *25*, 657–676.

Lai, R. J., S. R. Long, and N. E. Huang (1989), Laboratory studies of wave-current interaction: Kinematics of the strong interaction, *J. Geophys. Res.*, *94*(C11), 16,201–16,214.

Lake, B. M., H. C. Yuan, H. Rungaldier, and W. E. Ferguson (1977), Nonlinear deep-water waves: Theory and experiment: 2: Evolution of a continuous wave train, *J. Fluid Mech.*, *83*, 49–74.

Lavrenov, I. V. (1998), The wave energy concentration at the Agulhas current off South Africa, *Nat. Hazards*, *17*, 117–127.

Liu, P. C., and G. S. Miller (1996), Wavelet transforms and ocean current data analysis, *J. Atmos. Oceanic Technol.*, *13*(5), 1090–1099.

Liu, P. C., and U. F. Pinho (2004), Freak waves—More frequent than rare!, *Ann. Geophys.*, *22*(5), 1839–1842.

Longuet-Higgins, M. S. (1984), Statistical properties of wave groups in a random sea state, *Philos. Trans. R. Soc. London, Ser. A*, *312*, 219–250.

Mallory, J. K. (1974), Abnormal waves on the south-east of South Africa, *Inst. Hydrogr. Rev.*, *51*, 89–129.

Mei, C. C. (1983), *The Applied Dynamics of Ocean Surface Waves*, John Wiley, Hoboken, N. J.
Mori, N. (2004), Occurrence probability of a freak wave in a nonlinear wave field, *Ocean Eng.*, *31*, 165–175.
Mori, N., and T. Yasuda (2002), Effects of high-order nonlinear interactions on unidirectional wave trains, *Ocean Eng.*, *29*, 1233–1245.
Mori, N., P. C. Liu, and T. Yasuda (2002), Analysis of freak wave measurements in the Sea of Japan, *Ocean Eng.*, *29*, 1399–1414.
Myrhaug, D., and S. P. Kjeldsen (1986), Steepness and asymmetry of extreme waves and the highest waves in deep-water, *Ocean Eng.*, *13*, 549–568.
Nepf, H. M., C. H. Wu, and E. S. Chan (1998), A comparison of two- and three-dimensional wave breaking, *J. Phys. Oceanogr.*, *28*, 1496–1510.
Ochi, M. K., and C. H. Tasi (1983), Prediction of occurrence of breaking waves in deep water, *J. Phys. Oceanogr.*, *13*, 1482–1492.
Onorato, M., A. R. Osborne, M. Serio, and S. Bertone (2001), Freak waves in random ocean sea states, *Phys. Rev. Lett.*, *86*, 5831–5834.
Onorato, M., A. R. Osborne, and M. Serio (2002), Extreme wave events in directional, random oceanic sea states, *Phys. Fluids*, *14*(4), L25–L28.
Osborne, A. R., M. Onorato, and M. Serio (2000), The nonlinear dynamics of rogue waves and holes in deep-water gravity wave trains, *Phys. Lett. A*, *275*, 386–393.
Pelinovsky, E., T. Talipova, and C. Kharif (2000), Nonlinear-dispersive mechanism of the freak wave formation in shallow water, *Physica D*, *147*(1–2), 83–94.
Peregrine, D. H. (1976), Interaction of water waves and currents, *Adv. App. Mech.*, *16*, 9–117.
Peterson, P., T. Soomere, J. Engelbrecht, and E. van Groesen (2003), Soliton interaction as a possible model for extreme waves in shallow water, *Nonlinear Proc. Geophys.*, *10*(6), 503–510.
Rapp, R. J., and W. K. Melville (1990), Laboratory measurements of deep water breaking waves, *Philos. Trans. R. Soc. London, Ser. A*, *331*, 735–780.
Rosengaus Moshinsky, M. (1987), Experimental study of wave-generated bedforms and resulting wave attenuation, Ph.D. thesis, pp. 71–94, Mass. Inst. of Technol., Cambridge, Mass.
Sand, S. E., N. E. O. Hansen, P. Klinting, O. T. Gudmestad, and M. J. Sterndorff (1990), Freak wave kinematics, in *Water Wave Kinematics*, edited by A. Torum and O. T. Gudmestad, pp. 535–549, Kluwer Acad., Norwell, Mass.
Schlurmann, T. (2002), Spectral analysis of nonlinear water waves based on the Hilbert-Huang transformation, *J. Offshore Mech. Arct. Eng.*, *124*, 22–27.
Slunyaev, A., C. Kharif, E. Pelinovsky, and T. Talipova (2002), Nonlinear wave focusing on water of finite depth, *Physica D*, *173*, 77–96.
Smith, R. (1976), Giant waves, *J. Fluid Mech*, *77*, 417–431.
Soares, C. G., Z. Cherneva, and E. M. Antao (2004), Steepness and asymmetry of the largest waves in storm seas, *Ocean Eng.*, *31*, 1147–1167.
Stansberg, C. T. (1994), Effects from directionality and spectral bandwidth on nonlinear spatial modulations of deep-water surface gravity waves, in *Proceedings of the 24th International Conference on Coastal Engineering*, edited by B. Edge, pp. 579–593, Am. Soc. of Civ. Eng., Reston, Va.
Stansell, P., J. Wolfram, and S. Zachary (2003), Horizontal asymmetry and steepness distributions for wind-driven ocean waves from severe storms, *Appl. Ocean Res.*, *25*, 137–155.
Su, M. Y., M. Bergin, and R. Myrick (1982), Experiments on nonlinear instabilities and evolution of steep gravity wave, *J. Fluid Mech.*, *124*, 45–72.
Thomas, G. P., and G. Klopman (1997), Wave-current interactions in the nearshore region, in *Gravity Waves in Water of Finite Depth*, edited by J. N. Hunt, pp. 215–319, Comput. Mech., Billerica, Mass.
Trulsen, K., and K. B. Dysthe (1997), Freak waves—A three-dimensional wave simulation, in *Proceedings of the 21st Symposium on Naval Hydrodynamics*, pp. 550–560, Natl. Acad., Washington, D. C.
Tulin, M. P., and J. Li (1992), On the breaking of energetic waves, *Int. J. Offshore Polar Eng.*, *2*, 46–53.
Tulin, M. P., and T. Waseda (1999), Laboratory observations of wave group evolution, including breaking effects, *J. Fluid Mech.*, *378*, 197–232.
Veltcheva, A. D. (2002), Wave and group transformation by a Hilbert spectrum, *Coastal Eng. J.*, *44*, 283–300.
White, B. S., and B. Fornberg (1998), On the chance of freak waves at sea, *J. Fluid Mech.*, *355*, 113–138.
Wu, C. H., and H. Nepf (2002), Breaking criteria and energy losses for three-dimensional wave breaking, *J. Geophys. Res.*, *107*(C10), 3177, doi:10.1029/2001JC001077.
Yao, A., and C. H. Wu (2004), Energy dissipation of unsteady wave breaking on currents, *J. Phys. Oceanogr.*, *34*, 2288–2304.
Yasuda, T., and N. Mori (1997), Occurrence properties of giant freak waves in sea area around Japan, *J. Waterw. Port Coastal Ocean Eng.*, *123*(4), 209–213.

C. H. Wu and A. Yao, Department of Civil Environmental Engineering, University of Wisconsin-Madison, Madison, WI 53706, USA. (chinwu@engr.wisc.edu)